AIChE

Computational Study of Heat Transfer in a Bubbling Fluidized Bed with a Horizontal Tube

Q. F. Hou, Z. Y. Zhou, and A. B. Yu
Laboratory for Simulation and Modelling of Particulate Systems, School of Materials Science and Engineering, The University of New South Wales, Sydney, NSW 2052, Australia

DOI 10.1002/aic.12700
Published online July 20, 2011 in Wiley Online Library (wileyonlinelibrary.com).

A combined approach of discrete particle simulation and computational fluid dynamics is used to study the heat transfer in a fluidized bed with a horizontal tube. The approach is first validated through the good agreement between the predicted distribution and magnitude of local heat transfer coefficient with those measured. Then, the effects of inlet fluid superficial velocity, tube temperature and main particle properties such as particle thermal conductivity and Young's modulus are investigated and explained mechanistically. The relative importance of various heat transfer mechanisms is analyzed. The convection is found to be an important heat transfer mode for all the studied conditions. A large convective heat flux corresponds to a large local porosity around the tube, and a large conductive heat flux corresponds to a large number of particle contacts with the tube. The heat transfer is enhanced by the increase of particle thermal conductivity while it is little affected by Young's modulus. Radiative heat transfer becomes increasingly important as the tube temperature is increased. The results are useful for temperature control and structural design of fluidized beds. © 2011 American Institute of Chemical Engineers *AIChE J*, 58: 1422–1434, 2012
Keywords: discrete particle simulation, heat transfer, fluidization, horizontal tube

Introduction

Fluidization is widely used in industries as a major flow mode in chemical processes, due to its high heat and mass-transfer capability. Immersed surfaces such as horizontal/vertical tubes, fins and water walls are usually adopted in such processes to control flow and heat transfer. Understanding the flow and heat transfer mechanisms is important to achieve optimal design and control of fluidized systems.[1] Many studies have been carried out in this area, resulting in various empirical correlations for the heat transfer coefficient (HTC).[2–6] These correlations have shown their value in solving some practical problems. However, to produce equations that can be generally applied to different systems, microscopic understanding of the heat transfer mechanisms is important.

With this realization, the heat transfer between a single large particle and a fluidized/packed bed of small particles has recently been examined experimentally.[7–10] In these studies, a hot sphere is immersed in the bed, and its transient temperature is measured using an attached thermocouple. Some studies have focused on how the HTC of a tube is affected by the surrounding gas–solid flow characteristics such as particle residence time and porosity by means of: a heat-transfer probe, positron emission particle tracking (PEPT) method or an optical probe.[11–13] The variations in HTC with the probe position and fluid velocity were analyzed. The observed angular variation in HTC was explained by the PEPT data. While useful for fundamental understanding and model validation, such experimental studies have a difficulty in quantifying the contributions to heat transfer by the individual heat transfer modes, i.e., convection, conduction and radiation. Further complications arise from the fact that the heat transfer is strongly dependent on the local gas–solid flow structure and the interactions of various types, e.g., between particles and between particles and immersed surface. It is a challenging task to measure these spatially and temporally varying factors in relation to the HTC.

In recent years, discrete particle simulations (DPS) combined with computational fluid dynamics (CFD) becomes more and more popular in the studies of flow and heat transfer of particulate systems at a particle scale, as reviewed by Zhu et al.[14,15] Such methods can generate detailed microscopic information of the local flow structures and interactions of the particles with all other objects including fluids. The method has been successfully applied in the study of heat transfer and combustion in fluidized beds without an immersed surface.[16–19] In addition, attempts have also been made to apply the method to study the heat transfer in a fluidized bed with an immersed tube.[20,21] In particular, Di Maio et al.[20] compared different particle-to-particle heat-transfer models and suggested that the formulation of such models are important for obtaining simulation results comparable to experimental measurements. Zhao et al.[21] used an unstructured mesh suitable for a complex geometry and discussed the effects of particle diameter and superficial fluid velocity on the HTC at a low temperature. These studies demonstrate the applicability of the DPS-CFD approach to a fluidized bed with an immersed tube.

Correspondence concerning this article should be addressed to A. B. Yu at a.yu@unsw.edu.au.

However, some important aspects have not been considered in the previous two studies.[20,21] First, the bed geometry was only two-dimensional (2-D) with its thickness equal to one particle diameter. As recently pointed out by Feng and Yu,[22] a 3-D bed is more reliable to investigate the structure-related phenomena such as heat transfer. Second, the fluid properties such as fluid density and thermal conductivity were treated as constants. However, variations in these properties have a significant effect on heat transfer.[23,24] Third, although the particle–particle heat transfer has been proved to be critical to the generation of satisfactory results,[20] these studies did not consider separately the heat transfer mechanisms associated with static and collisional contacts.[17] Finally, the radiative heat transfer mode was ignored, which will, however, make a significant contribution to heat transfer at high temperatures.[1,25–27] There is a need to overcome these gaps, and examine the heat transfer problem under different conditions more carefully.

In this work, in connection with our previous attempt,[28] the combined approach of DPS and CFD proposed by Zhou et al.[17] will be extended to investigate the heat transfer in a 3-D gas-fluidized bed with an immersed horizontal tube. The fluid properties are temperature-dependent, and all the heat transfer modes such as conduction, convection and radiation are explicitly considered. The proposed model will be first tested against the experimental results in the literature. Then it will be used to investigate the effects of inlet fluid superficial velocity, tube temperature and other main particle properties on the heat transfer in a fluidized bed.

Model Description

Governing equations for solid phase

Here, the solid phase is treated as a discrete phase, and its motion is described by the discrete element method (DEM) originally proposed by Cundall and Strack.[29] A particle in a fluidized bed has two types of motion: translational and rotational. During its motion, the particle may interact with its neighboring particles, tubes/walls, and the surrounding fluid. The momentum and energy are exchanged through these interactions. At any given time t, the equations governing the translational and rotational motions of particle i in a gas–solid two-phase flow system can be written as

$$m_i d\mathbf{v}_i/dt = \sum_j (\mathbf{f}_{e,ij} + \mathbf{f}_{d,ij}) + \mathbf{f}_{pf,i} + m_i\mathbf{g} \tag{1}$$

and

$$I_i d\boldsymbol{\omega}_i/dt = \sum_j (\mathbf{T}_{t,ij} + \mathbf{T}_{r,ij}) \tag{2}$$

where $\mathbf{v}_i$ and $\boldsymbol{\omega}_i$ are the translational and rotational velocities of the particle, respectively. The forces involved are: the gravitational force $m_i\mathbf{g}$, interparticle forces which include elastic force $\mathbf{f}_{e,ij}$ and viscous damping force $\mathbf{f}_{d,ij}$, and particle-fluid interaction force $\mathbf{f}_{pf,i}$ which mainly includes the drag force $\mathbf{f}_{d,i}$ and pressure gradient force $\mathbf{f}_{pg,i}$. These interparticle forces can be resolved into the normal and tangential components at a contact point. The torque acting on particle i by particle j includes two components: $\mathbf{T}_{t,ij}$ which is generated by tangential force and causes particle i to rotate, and $\mathbf{T}_{r,ij}$ which, commonly known as the rolling friction torque, is generated by asymmetric normal forces and slows down the relative rotation between particles. For a particle undergoing multiple interactions, the individual interaction forces and torques are summed over all the particles interacting with particle i. The equations used to calculate the particle–particle interaction forces and torques, and particle-fluid interaction forces are listed in Table 1. Most of the equations have been well established, as for example, reviewed by Zhu et al.[15] Note that the sets of equations for DEM and CFD approaches should be consistent with each other, this also including the equation for the calculation of particle-fluid interaction force.[30,31] ϵ_i is the local porosity for particle i to calculate particle-fluid drag force and ϵ_f is determined over a computational cell for fluid phase. Theoretically, the two porosities should be calculated separately. However, for this work, they have the same definition and given by $\varepsilon_i = 1 - \sum_{i=1}^{k_v} V_i/\Delta V$.

Table 1. Equations to Calculate the Forces and Torques on Particle *i*

Force or torque	Equation
Normal elastic force, $\mathbf{f}_{en,ij}$	$-\frac{4}{3}E^*\sqrt{R^*}\delta_n^{3/2}\mathbf{n}$
Normal damping force, $\mathbf{f}_{dn,ij}$	$-c_n\left(6m_{ij}E^*\sqrt{R^*\delta_n}\right)^{1/2}\mathbf{v}_{n,ij}$
Tangential elastic force, $\mathbf{f}_{et,ij}$	$-\mu_s\lvert\mathbf{f}_{en,ij}\rvert\left(1-(1-\delta_t/\delta_{t,\max})^{3/2}\right)\hat{\boldsymbol{\delta}}_t$
Tangential damping force, $\mathbf{f}_{dt,ij}$	$-c_t\left(6\mu_s m_{ij}\lvert\mathbf{f}_{en,ij}\rvert\sqrt{1-\delta_t/\delta_{t,\max}}/\delta_{t,\max}\right)^{1/2}\mathbf{v}_{t,ij}$
Coulomb friction force, $\mathbf{f}_{t,ij}$	$-\mu_s\lvert\mathbf{f}_{en,ij}\rvert\hat{\boldsymbol{\delta}}_t$
Torque by tangential forces, $\mathbf{T}_{t,ij}$	$\mathrm{R}_{ij}\times\left(\mathbf{f}_{et,ij}+\mathbf{f}_{dt,ij}\right)$
Rolling friction torque, $\mathbf{T}_{r,ij}$	$\mu_r\lvert\mathbf{f}_{en,ij}\rvert\hat{\boldsymbol{\omega}}_{ij}^n$
Particle-fluid drag force, $\mathbf{f}_{d,i}$	$0.125C_{d_{0,i}}\rho_f\pi d_{pi}^2\varepsilon_i^2\lvert\mathbf{u}_i-\mathbf{v}_i\rvert(\mathbf{u}_i-\mathbf{v}_i)\varepsilon_i^{-\chi}$
Pressure gradient force, $\mathbf{f}_{pg,i}$	$-\nabla p_i\cdot V_i$

where $1/m_{ij}=1/m_i+1/m_j$, $1/R^*=1/\lvert\mathbf{R}_i\rvert+1/\lvert\mathbf{R}_j\rvert$, $E^*=E/2(1-\nu^2)$, $\hat{\boldsymbol{\omega}}_{ij}^n=\boldsymbol{\omega}_{ij}^n/\lvert\boldsymbol{\omega}_{ij}^n\rvert$, $\hat{\boldsymbol{\delta}}_t=\boldsymbol{\delta}_t/\lvert\boldsymbol{\delta}_t\rvert$, $\delta_{t,\max}=\mu_s\delta_n(2-\nu)/(2(1-\nu))$, $\mathbf{v}_{ij}=\mathbf{v}_j-\mathbf{v}_i+\boldsymbol{\omega}_j\times\mathbf{R}_j-\boldsymbol{\omega}_i\times\mathbf{R}_i$, $\mathbf{v}_{n,ij}=(\mathbf{v}_{ij}\cdot\mathbf{n})\cdot\mathbf{n}$, $\mathbf{v}_{t,ij}=(\mathbf{v}_{ij}\times\mathbf{n})\times\mathbf{n}$, $\chi=3.7-0.65\exp[-(1.5-\log_{10}\mathrm{Re}_i)^2/2]$, $C_{d0,i}=(0.63+4.8/\mathrm{Re}_i^{0.5})^2$, $\mathrm{Re}_i=\rho_f d_{pi}\varepsilon_i\lvert\mathbf{u}_i-\mathbf{v}_i\rvert/\mu_f$, $\varepsilon_i=1-\sum_{i=1}^{k_v}V_i/\Delta V$.
Note that tangential forces ($\mathbf{f}_{et,ij}+\mathbf{f}_{dt,ij}$) should be replaced by $\mathbf{f}_{t,\ ij}$ when $\delta_t \geq \delta_{t,\max}$.

The heat transfer of particle i and its surroundings generally has three modes: convection with fluid; conduction with other particles, walls and tube; and radiation with its local surrounding environment. According to the energy balance, the governing equation for particle i can be written as[17]

$$m_i c_{p,i} dT_i/dt = \sum_j q_{i,j} + q_{i,f} + q_{i,rad} + q_{i,wall} + q_{i,tube} \tag{3}$$

where $q_{i,j}$ is the conductive heat flux between particles i and j, $q_{i,f}$ is the convective heat flux between particle i and its local surrounding fluid, $q_{i,\mathrm{rad}}$ is the radiative heat flux between particle i and its local surrounding environment, $q_{i,\mathrm{tube}}$ is the conductive heat flux between particle i and tube, and $q_{i,\mathrm{wall}}$ is the conductive heat flux between particle i and wall. Mathematically, Eq. 3 is the same as the so-called lumped-capacity formulation, where the thermal resistance within a particle can be neglected.[32] This condition is reasonable when the Biot number, defined as $h\cdot(V_i/A_i)/k_{pi}$, is less than 0.1. However, as noted by Zhou et al.[17] Eq. 3 is established on the basis of energy balance at the particle scale. So, the values of the parameters (e.g., m_i, c_{pi}, T_i, and k_{pi}) involved should be the representative properties of the particle at this scale. So is the

Table 2. Equations to Calculate Heat Fluxes

Heat flux	Equation
Convective	$q_{i,f} = (2.0 + a\mathrm{Re}_i^b \mathrm{Pr}^{1/3}) k_f A_i \Delta T / d_{pi}$
	$q_{f,wall} = 0.037\mathrm{Re}^{0.8} \mathrm{Pr}^{1/3} k_f A_w \Delta T / L$
Conductive	$q_{i,j} = (T_j - T_i) \int_{r_{sij}}^{r_{sf}} 2\pi \cdot r((\sqrt{R^2 - r^2} - r(R+H)/r_{ij}) \cdot (1/k_{pi} + 1/k_{pj}) + 2[(R+H) - \sqrt{R^2 - r^2}]/k_f)^{-1} dr$ (a)
	$q_{i,j} = 4r_c(T_j - T_i)/(1/k_{pi} + 1/k_{pj})$ (b)
	$q_{i,j} = c(T_j - T_i)\pi r_c^2 t_c^{-1/2} / ((\rho_{pi} c_{pi} k_{pi})^{-1/2} + (\rho_{pj} c_{pj} k_{pj})^{-1/2})$ (c)
Radiative	$q_{i,rad} = \sigma e A_i (T_{local,i}^4 - T_i^4)$, $q_{f,rad} = \sigma e_f A_f (T_{local,i}^4 - T_f^4)$
	where $T_{local,i} = \varepsilon_i T_{f,\Omega} + (1 - \varepsilon_i) \sum_{j=1}^{k_\Omega} T_j (j \neq i)/k_\Omega$

case for the equations used to calculate the heat fluxes involved.

The equations to calculate the heat fluxes in Eq. 3 are listed in Table 2, and these equations have been discussed and used by Zhou et al.[17,33] Note that Eq. (a) in the table is for the conductive heat flux through fluid between particles i and j;[34,35] Eqs. (b) and (c) are, respectively, for the conduction through static solid contacts area or the solid contact area due to collisions.[36–38] As used in the previous work,[17] two parameters are set to distinguish these two mechanisms: particle–particle collision time t_c and particle–particle contact duration time t_d. For two colliding particles, if $t_c \geq t_d$, only collisional heat transfer applies. If $t_c < t_d$, two particles will keep in touch after collision. In such a case, collision heat transfer applies first during the time of t_c, and then static heat transfer during the time of $(t_d - t_c)$. The conduction between a tube and a particle is considered in a similar manner to that between particles. The equation for the local convection between the tube and fluid is the same as between a wall and fluid. In this study, these equations are extended to include the heat transfer between a tube and particles or fluid. The tube is here treated as a wall because its size is much larger than a particle or a computational cell used in CFD; otherwise, it can be treated as a particle. In fixed and fluidized beds, a particle in the bed is surrounded by other particles and fluid. For each particle, an isolated domain is chosen to be its environment so that $q_{i,\mathrm{rad}}$ can be evaluated by the model for gray bodies.[1,17] In the specified enclosed domain, the local environmental temperature ($T_{\mathrm{local},i}$) is assumed to represent the surface temperature of the enclosure around such a particle. The radiation between a tube and a fluidized bed is similarly considered. This consideration for the radiative heat-transfer mode is reasonable, at least in packed or bubbling fluidized beds where most of particles are in a relatively closely packed state. With a proper domain size for the considered system, a particle/tube could be fully enclosed. For this study, the domain size for the radiative heat transfer between particles is the same as a computational cell ($2d_\mathrm{p}$). The definition of bed temperature (T_b), and tube environmental temperature (T_e), are the same as $T_{\mathrm{local},i}$ in the equations given in Table 2. The local porosity and T_e in the vicinity of the tube are obtained for an annular region around the tube with a thickness of $5d_\mathrm{p}$ in its radial direction. Furthermore, to examine the local HTC of a tube, the circumference of the tube is evenly divided into 16 sections. The local contact number is the number of particles contacting a section of the tube. The overall heat flux and contact number are the sum of all sections, and the overall porosity is the average of all sections.

Governing equations for fluid phase

The fluid phase, air to be specific for this study, is treated as a continuum phase and modeled in a similar manner to the widely used conventional two-fluid modeling.[39] Thus, the governing equations for the fluid phase are the conservations of mass and momentum, which are expressed in terms of the local average variables over a computational cell, given by

$$\partial(\rho_f \varepsilon_f)/\partial t + \nabla \cdot (\rho_f \varepsilon_f \mathbf{u}) = 0 \tag{4}$$

$$\partial(\rho_f \varepsilon_f \mathbf{u})/\partial t + \nabla \cdot (\rho_f \varepsilon_f \mathbf{u}\mathbf{u}) = -\nabla p - \mathbf{F}_{fp} + \nabla \cdot \tau + \rho_f \varepsilon_f \mathbf{g} \tag{5}$$

The corresponding energy equation for heat transfer can be written as:

$$\partial(\rho_f \varepsilon_f c_{pf} T)/\partial t + \nabla \cdot (\rho_f \varepsilon_f \mathbf{u} c_{pf} T) = \nabla \cdot (k_e \nabla T) + Q \tag{6}$$

where $\mathbf{u}$, ρ_f, p and $\mathbf{F}_{fp}$ are the fluid velocity, density, pressure and volumetric fluid-particle interaction force, respectively τ $(= \mu_e[(\nabla \mathbf{u}) + (\nabla \mathbf{u})^{-1}] - 2\mu_e(\nabla \cdot \mathbf{u})\delta_k/3)$ and ϵ_f $(= 1 - \sum_{i=1}^{k_v} V_i/\Delta V)$ are the fluid viscous stress tensor and porosity, respectively, with V_i representing the volume of particle i (or part of the volume if the particle is not fully in a CFD cell), and k_V the number of particles in the computational cell of volume ΔV. Furthermore, μ_e $(= \mu_f + C_\mu \rho_f \epsilon_f k^2/\epsilon)$ is the fluid effective viscosity and μ_t is the turbulent viscosity, which are determined by a widely used standard k-ϵ turbulence model.[17,40,41] The turbulence of the solid phase is not considered, and this treatment has been tested as acceptable for systems with large particles.[42] k_e is the effective fluid thermal conductivity, defined by $(k_f + c_{pf}\mu_t/\sigma_T)$, and σ_T the turbulence Prandtl number, which is set to 1.00 for this work. The volumetric particle-fluid interaction force $\mathbf{F}_{fp}$ in Eq. 5 can be determined as $\mathbf{F}_{fp} = \sum_{i=1}^{k_v} (\mathbf{f}_{d,i} + \mathbf{f}_{pg,i})/\Delta V$. The volumetric heat flux Q in Eq. 6 can be determined as $Q = (\sum_{i=1}^{k_v} q_{f,i} + q_{f,wall} + q_{f,tube} + q_{f,rad})/\Delta V$, where $q_{f,i}$ is the convective heat flux between fluid and particle i, $q_{f,\mathrm{tube}}$ is the convective heat flux between fluid and a tube, $q_{f,\mathrm{wall}}$ is the convective heat flux between fluid and a wall, and $q_{f,\mathrm{rad}}$ is the radiative heat flux between fluid and its environment. In this work, because of the low emissivity of fluid, the radiative heat transfer between fluid and its environment is ignored for simplicity. The equations to calculate these heat fluxes are given in Table 2.

HTC represents the possible heat transfer capability, and depends on its definition and associated concepts such as the temperature difference and the effective surface area while a heat flux is a real energy exchange. The trends of variations of HTC and heat flux may not always be the same if each is expressed as a function of the parameters such as inlet fluid superficial velocity, particle thermal conductivity and Young's modulus of the particles. The local HTC of a

section is determined as $h = (q_{conv} + q_{cond} + q_{rad})/A/(T_s - T_b)$, where q_{conv} is the local convective heat flux between the tube and fluid; q_{cond} is the local conductive heat flux between the tube and particles; q_{rad} is the local radiative heat flux between the tube and its surrounding environment, A is the surface area of a section, T_s is the tube temperature, and T_b is the bed temperature.

Heat flux and HTC of the tube vary with time. The heat fluxes due to conduction, convection and radiation increase first in the heating up process because of the large temperature difference in the bed and then, decrease because of the increase of the uniformity of the temperature field. Therefore, averaged values of heat fluxes are obtained within a fixed time frame (0–6 s) to be comparable.

DPS-CFD coupling scheme

The methods of numerical solutions to problems requiring DPS-CFD coupling have been well established.[31,43,44] The heat transfer model has also been implemented into this approach as demonstrated for a bubbling fluidized bed.[17] This work extends this approach further to consider an immersed tube in a fluidized bed, between which heat transfer occurs. The coupling scheme used here is the same as before, and can be briefly described as follows for completeness. At each time step, DPS will produce information such as the positions, velocities, and temperature of individual particles, which will be used for the evaluation of porosity, particle-fluid interaction force, and heat flux in a computational cell. CFD will then use this information to determine the fluid flow and temperature field, which in turn can be used to find the particle-fluid interaction force and heat transfer between fluid and particles or the tube. Incorporation of the resulting forces and heat fluxes into DPS will produce information about the motion and temperature of individual particles for the next time step.

Simulation conditions

Table 3 lists the physical and geometrical parameters used in this work, where the varying ranges of particle and bed parameters are in bracket. This work is also concerned with the effects of some important parameters. For simplicity, we vary one of these properties while the rests assume the default base values. For the DPS model, particles and walls are assumed to have the same properties for convenience. Spherical particles are used as the solid phase fluidized in a container with a thickness of $4d_p$. The periodic boundary condition is applied to the front and rear direction to eliminate the effect of corresponding walls. For a bed whose width is much larger than its thickness, the combination of 3-D DPS and 2-D CFD is reasonable, as demonstrated by Feng et al.[44] The nonslip boundary condition is applied to the container walls, and zero diffusion flux condition to the outlet. A uniform mesh, although not perfect for tubes, is used as done by other investigators.[45,46] After some trial tests, a cell size of $2d_p$ is selected for the system considered.

The simulations are started with the random generation of particles without overlap in the cuboid bed, followed by a gravitational settling process. The particles are allowed to settle until the rotational and translational velocities of the particles decay to zero. The bed so generated is then used as a starting point for various simulations, and to fluidize the particles, air at a pre-set superficial velocity and ambient temperature is uniformly injected from the bottom of the bed. The temperature of the tube is assumed to be constant, and the container walls to be adiabatic.

Table 3. Physical and Geometrical Parameters Used in the Simulations

Variables	Default and varying range in bracket
Bed width × height, mm	60 × 768
Tube position (Z), mm	30
CFD cells, -	50 × 640
Cell size ($\Delta x \times \Delta z$), mm	1.2 × 1.2
Number of particles (N), -	30000
Tube diameter, mm	24
Particle diameter d_p, mm	0.6
Particle density ρ_p, kg/m^3	2600
Thermal conductivity of particle k_p, W/(m·K)	1.1 (1.1∼300)
Thermal conductivity of tube k_{pt}, W/(m·K)	380
Heat capacity of particle c_p, J/(kg·K)	840.0
Heat capacity of the tube c_{pt}, J/(kg·K)	24.4
Initial temperature of particles and air, °C	25
Temperature of tube, °C	100 (100∼1500)
Particle-particle/wall sliding friction μ_s, -	0.30
Particle-particle/wall rolling friction μ_r, -	0.01
Restitution coefficient, -	0.80
Particle Young's modulus E, MPa	10 (1∼1000)
Particle poisson ratio v, -	0.30
Time step Δt, s	1×10^{-5}
Fluid density ρ_f, kg/m^3	$PM/(RT_f)$
Fluid molecular viscosity μ_f, Pa·s	$1.511 \times 10^{-6} T_f^{3/2}/(T_f + 120.0)$
Fluid thermal conductivity k_f, W/(m·K)	$2.873 \times 10^{-3} + 7.760 \times 10^{-5} \times T_f$
Fluid specific heat capacity c_{pf}, J/(kg·K)	$1002.737 + 1.232 \times 10^{-2} \times T_f$

Results and Discussion

Model validation

The particle and tube properties are listed in Table 3, and simulation conditions are based on the experimental investigation by Wong and Seville.[12] Since the heat transfer between the tube and the fluidized bed is affected mainly by the vicinal environment of the tube,[47] a smaller bed is used to reduce the computational effort. Such a strategy allows us to make meaningful comparisons between predicted and measured results. The excess fluid velocity (u_{exc}) in the following discussion is defined as the difference between the superficial fluid velocity (u) at the inlet and minimum fluidization velocity (u_{mf}). The validation is carried out in terms of flow patterns and local HTC distribution. The predicted value of $u_{mf} = 0.27$ m/s are consistent with the experimental measurements.[12,48] The bubbling fluidized bed behavior is significantly affected by the insertion of the horizontal tube. The behavior can be generally characterized by two main features: a defluidized region downstream and an air film upstream of the flow.[12,46,49] As shown in Figure 1, these characteristics are successfully captured by the simulations. The particles are colored by coordination number[50,51] (CN, which is the number of particles in contact with a given particle) of individual particles which is closely related to the conductive heat transfer. Particles with small velocities tend to stay on the tube at downstream where CN is large (as seen from the snapshot at $t = 0.2$ s in Figure 1), and the

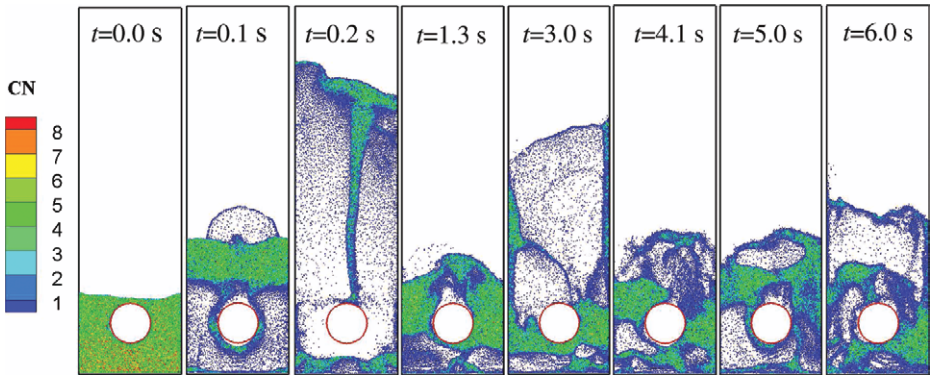

Figure 1. Snapshots of solid flow patterns colored by CN when u_{exc} = 0.50 m/s.

[Color figure can be viewed in the online issue, which is available at wileyonlinelibrary.com.]

defluidized region is formed intermittently. An air film is formed below the tube at upstream, and its thickness varies with time. The upstream section can be fully filled with particles sometimes (e.g., t = 1.3 s and 3.0 s in Figure 1).

The tube exchanges heat with its surrounding environment. Local HTC has a distribution closely related to the particle flow patterns. The distribution and magnitude of HTC are two factors commonly used to describe the heat transfer in the system.[2,12,52] Figure 2 shows a comparison of the effects of u and tube position Z on the local HTC, determined by experiments[12] and these simulations. Predictions by the simulations agree reasonably well with the measurements in three aspects. First, the local HTC is high at the tube sides around 90 and 270°, and low around 0 and 180° at upstream and downstream. The predicted trends agree also with the measurements by others.[2,11] The magnitude of the maximum HTC also matches the measurements satisfactorily. Second, the effect of u is qualitatively consistent with the measurements: an increase of u will increase the local HTC to a maximum and then reduce it (Figure 2a). Third, the predicted effect of tube position Z agrees well with measurements: the local HTC increases with an increase in Z (Figure 2b). The consistencies in the results suggest that the proposed model can be used to study the heat transfer between a fluidized bed and a tube at least qualitatively, although some treatments in the DPS-CFD approach are still not perfect at this stage of the development.

Overall and local heat fluxes at a low temperature

At low temperatures, heat is transferred mainly through the convection between fluid and particles and between fluid and the tube, and the conduction among particles and between particles and tube; the radiative heat transfer is not discussed in this section because it is quite small at low temperatures. To demonstrate this point, Figure 3 shows the overall heat fluxes through convection and conduction, respectively and the corresponding porosity and contact number when u_{exc} = 0.40 m/s. The values of convective and conductive heat fluxes vary with time, with the convective heat flux showing a larger value than the conductive one. The percentage of the convective heat transfer is dominant over the conduction with a percentage of over 90% for the system considered.

As shown in Figure 3, the heat fluxes are closely related to the microstructure around the tube. Note that the overall values of porosity around the tube and contact number between the tube and particles can be used to index the microstructure around the tube. The porosity and contact number vary temporally as a result of the complicated interactions between the tube and particles, and between particles and fluid. Generally, a region with a large contact number corresponds to a defluidized region in the vicinity of the tube with a small porosity. In that region, the conductive heat flux is large, and there is a correspondence between the peaks in the curves of conductive heat flux and contact

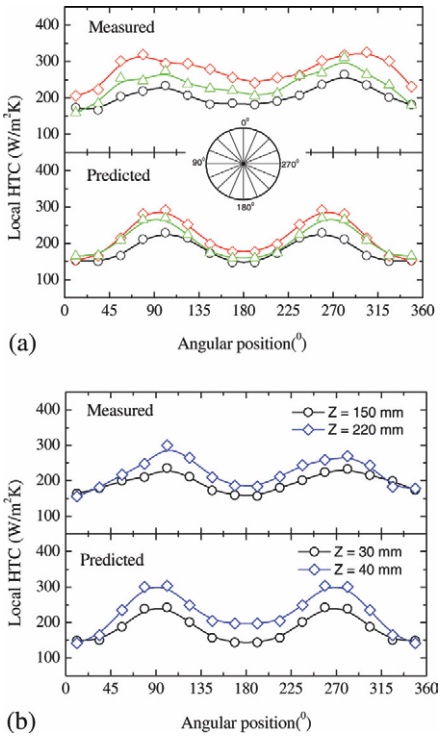

Figure 2. Comparisons of local HTC distribution (a) at different u_{exc} (○, 0.08 m/s; ◇, 0.50 m/s; △, 0.80 m/s; and the inset shows the angular division), and (b) at different Z when u_{exc} = 0.20 m/s.

The measurements are from Wong and Seville.[12] [Color figure can be viewed in the online issue, which is available at wileyonlinelibrary.com.]

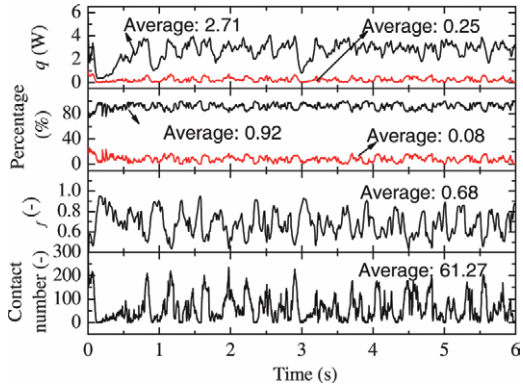

Figure 3. Evolution of overall convective and conductive heat fluxes (q) and their percentages (-, convection; −, conduction), overall porosity (ϵ_f) and contact number when u_{exc} = 0.40 m/s.

[Color figure can be viewed in the online issue, which is available at wileyonlinelibrary.com.]

number. A low heat flux corresponds to a passing bubble, where the porosity is large and the contact number is small. When a bubble passes, the convective heat flux is large due to the large porosity in the passing bubble. These results are consistent with the particle flow patterns shown in Figure 1.

HTC is not uniform around the tube as shown in Figure 2. Thus, it is necessary to examine the local heat-transfer characteristics, which are closely related to the local gas–solid flow structures around the tube. Here the focus is the effects of contact number and porosity. Figure 4 shows the variations of conductive (q_{cond}), and convective (q_{conv}) heat fluxes, the corresponding local porosity (ϵ_f) and contact number for the three representative sections: upstream, downstream and sides. The upstream section has the largest conductive and the smallest convective heat flux, which corresponds to the largest contact number and the smallest porosity. This condition results in a small local HTC in the upstream section (around 180°) as shown in Figure 2. In addition, the large contact number around the tube has an adverse effect: the contact forces between particles and tube cause the erosion of the tube and, hence, its ultimate failure.[53] From this point of view, the micromechanical analysis is very useful for structural design of a fluidized bed. The downstream section has the smallest conductive heat flux corresponding to the smallest contact number, and has a moderately large convective heat flux corresponding to the largest porosity. The side sections with both moderately large contact number and porosity have a moderate conductive heat flux and the largest convective heat flux. It should be noted that the convective heat transfer is not only related to the local porosity but also the local fluid velocity. Having a larger fluid velocity than the downstream section, the side section with a moderately large porosity has the largest convective heat flux. Consequently, a smaller local HTC around 0° and a larger local HTC around 90 and 270° are observed as shown in Figure 2.

Clearly, the heat transfer between an immersed tube and a fluidized bed depends on many factors, such as the contacts of particles with the tube, porosity and fluid flow around the tube. These factors are affected by many variables related to operational conditions and material properties. Some of these effects are studied in this work, as reported in the following subsections.

Effect of inlet fluid superficial velocity u

u is one of the most important parameters affecting the heat transfer in a fluidized bed. Figure 2a has shown that the overall HTC increases with the increase of u_{exc} from 0.08 to 0.50 m/s, but decreases from 0.50 to 0.80 m/s. Here we examine the behavior of the heat flux in this velocity range, and the results are shown in Figure 5. It can be seen that for the system considered, the heat flux by convection is dominant and increases with the increase of u_{exc}. Although the heat flux by conduction decreases, the total heat flux increases continuously. Note that although the HTC decreases when $u_{exc} > 0.50$ m/s, the total heat flux does not decrease but increases gradually. The monotonous increase of the heat flux is because a large u_{exc} can here generate a large temperature difference between the fluidized bed and tube. This means that although a large u_{exc} can increase the heat transfer flux between the bed and tube, the uniformity of the temperature field of the bed could be deteriorated. Based on the variation of HTC with u_{exc}, a suitable u_{exc}

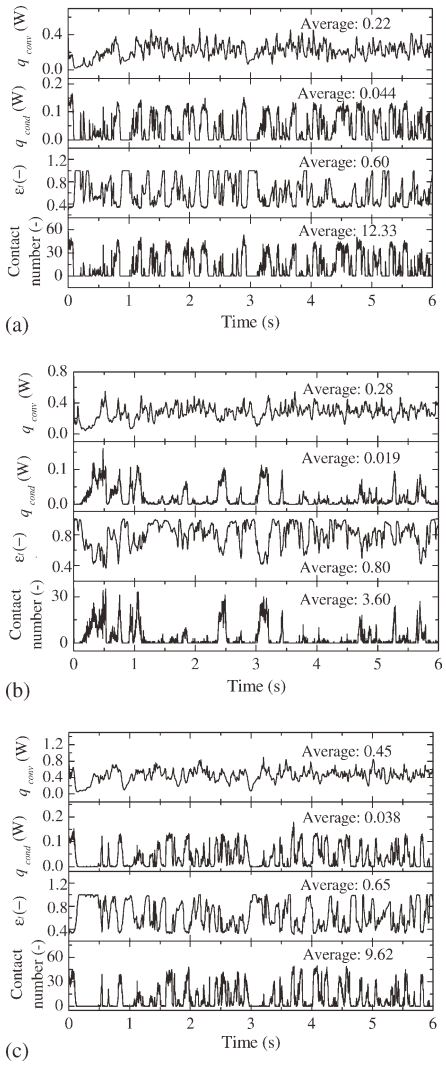

Figure 4. Evolution of local convective (q_{conv}) and conductive (q_{cond}) heat fluxes, local porosity (ϵ_f) and contact number (a) upstream (180 ± 22.5°), (b) downstream (0 ± 22.5°), and (c) sides (90 ± 22.5°) when u_{exc} = 0.40 m/s.

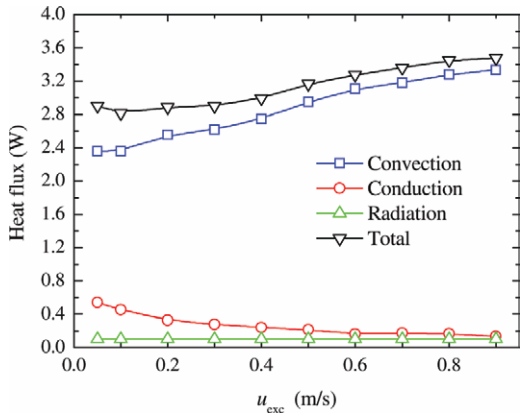

Figure 5. Heat fluxes as a function of u_{exc}.

[Color figure can be viewed in the online issue, which is available at wileyonlinelibrary.com.]

should be selected carefully to maximize the benefits in application.

The variations of porosity and contact number with u_{exc} are then examined as shown in Figure 6. Their time-averaged values are made for a given time frame (0–6 s), as mentioned earlier. Figure 6a shows that the time-averaged local porosity is large at the downstream and small at the upstream, while local contact number has an opposite distribution. The local porosity increases with the increase of u_{exc} and the local contact number decreases. The HTC is mainly affected by the convective heat transfer mode related to the local fluid velocity and porosity. The local fluid velocity around the tube is very complicated and has a distribution generally similar to the distribution of the local HTC.

Figure 6b shows the variations of time-averaged overall porosity and overall contact number at different u_{exc}. The time-averaged overall porosity increases with the increase of u_{exc}. Hence, the local Re increases. This explains why the convective heat transfer increases with the increase of u_{exc}. It also shows that the time-averaged overall contact number decreases with the increase of u_{exc}. It explains the decrease of the conductive heat transfer with the increase of u_{exc}. In fact, conductive heat transfer is also related to the properties such as the contact area of colliding particles with the tube.

According to this model, the conduction between particles and the tube involves several mechanisms including (1) particle-fluid-tube conductive heat transfer under either contact or non-contact conditions, and (2) particle-tube conductive heat transfer through either static or collisional solid contacts area. Their percentages can be used to quantify the effect of u on the conductive mechanisms, and the results are shown in Figure 7. It can be observed that the conduction through the particle-fluid-tube path under non-contact condition is dominant, followed by the contact condition. The conduction through particle-tube path is relatively small. This is because there are few contacts between particles and the tube. With the increase of u_{exc}, the conduction through particle-fluid-tube path under non-contact condition increases while the direct contact heat transfer (including static and collisional contact modes) decreases slightly. These findings show that gas film should be considered as an important factor affecting the heat transfer between particles and a tube. In fact, the conductive heat transfer can also be affected by the tube and particle properties, and will be discussed in the following subsections.

Effects of particle thermal conductivity k_p and Young's modulus E

k_p and E are two important particle properties affecting the heat transfer,[17,33] and their effects on heat transfer

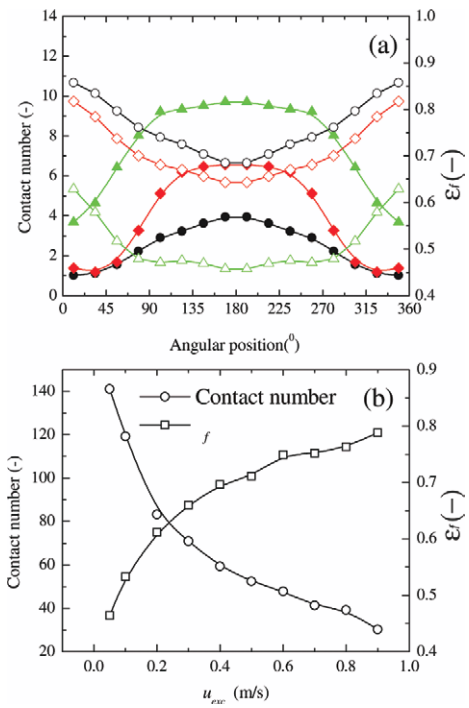

Figure 6. (a) time-averaged local porosity (open symbols) and local contact number (solid symbols) at different u_{exc} (▲, 0.08 m/s; ◆, 0.50 m/s; and ●, 0.80 m/s), and (b) time-averaged overall porosity (□) and overall contact number (○) as a function of u_{exc}.

[Color figure can be viewed in the online issue, which is available at wileyonlinelibrary.com.]

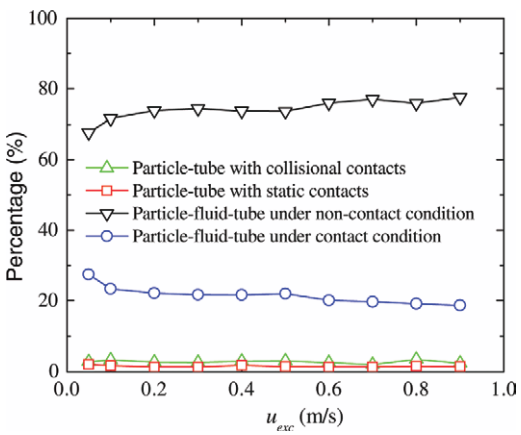

Figure 7. Percentages of heat fluxes in the conduction heat transfer by different conductive mechanisms at different u_{exc}.

[Color figure can be viewed in the online issue, which is available at wileyonlinelibrary.com.]

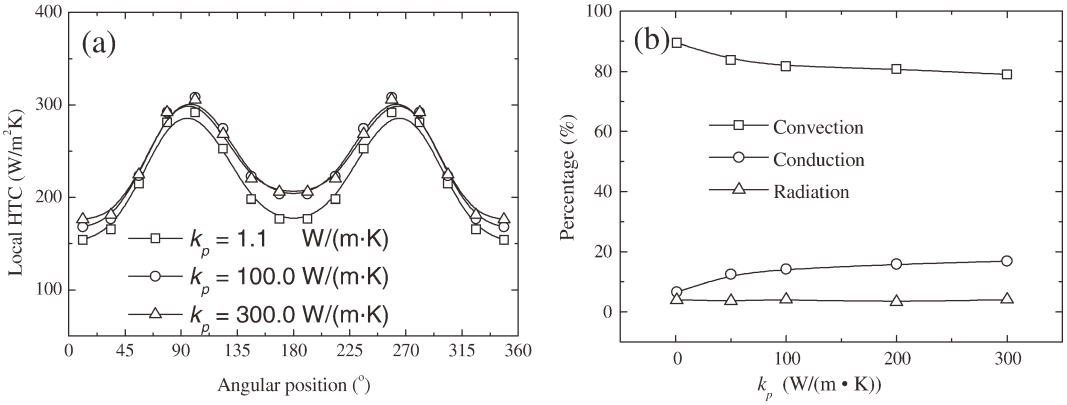

Figure 8. (a) local HTC, and (b) the percentages of heat fluxes by different heat-transfer modes as a function of k_p when u_{exc} = 0.50 m/s.

between the fluidized bed and tube are examined here. Figure 8a shows that the local HTC increases with the increase of k_p from 1.10 to 100 W/(m·K). However, there is no significant increase of HTC when k_p increases further from 100 to 300 W/(m·K). This result is expected because the heat transfer between the fluidized bed and the tube is mainly through the convective heat transfer mode, while k_p mainly affects the conductive heat transfer mode. Therefore, increasing k_p as a means of enhancing the heat transfer between a fluidized bed and a tube is not so significant.

Figure 8b examines the effect of k_p on the heat fluxes due to different heat transfer modes expressed as percentage contributions to the total heat flux. The percentage of the conductive heat flux increases with an increase of k_p and that of the convective heat flux decreases slightly when k_p is lower than 100 W/(m·K); a further increase of k_p has only a negligible effect. The convective heat flux continues to be dominant within the considered range of k_p. The effect of k_p on HTC is not significant as shown in Figure 8a.

Contributions by different conductive mechanisms to the total conductive heat transfer are examined below. Figure 9 shows the percentages of the heat flux due to several conductive mechanisms to the total conductive heat flux as a function of k_p. The percentage of the heat flux through the particle-fluid-tube path under non-contact condition decreases, while that through the particle-tube path with static contacts increases. The other two mechanisms are only slightly affected by k_p. When k_p is approximately over 150 W/(m·K), the heat flux by static contacts becomes larger than that through the particle-fluid-tube path under non-contact condition. These results show that the conductive heat transfer is complicated, and the roles of the mechanisms considered vary with k_p. In general, at low k_p, the heat flux although the particle-fluid-tube under non-contact conditions is dominant, and the gas film plays an important role in this case. When k_p is large, the heat transfer by static contacts becomes equally important.

Figure 10 shows the effect of E on different heat transfer modes. Figure 10 shows that E has a negligible effect on the local HTC in the range considered. Note that E mainly affects the contact area between particles and the tube and, thus, it affects the heat transfer by conduction. However, it was shown before that the convective heat transfer is the dominant mode of heat transfer between fluid and the tube for the process. The convection has been shown to be mainly related to gas–solid flow and not affected much by E.[33] Such evidence is further obtained from Figure 10b, where the percentages of heat fluxes due to different heat transfer modes are shown. The figure shows that the convective heat transfer changes little with E, but it does affect the conductive heat transfer to some degree. The total conductive heat flux and the percentages of heat fluxes due to different conductive mechanisms are shown as a function of E in Figure 11. The total conductive heat flux decreases slightly with the increase of E because of the decrease of particle-tube contact time and area. With the increase of E, and the accompanying reduction in the particle contact time, there will be more particles near the tube with the non-contacting conditions. Hence, the percentage of heat flux through the particle-fluid-tube path under non-contact condition increases while that of contact condition decreases. Figure 11 also shows that E has a negligible effect on the heat transfer through the contact area between particles and the tube.

From the aforementioned discussion, the dominant convective heat transfer mode is only slightly affected by the particle properties considered. However, these properties may affect significantly the conductive heat-transfer mode. Hence, in the study of heat transfer between a fluidized bed

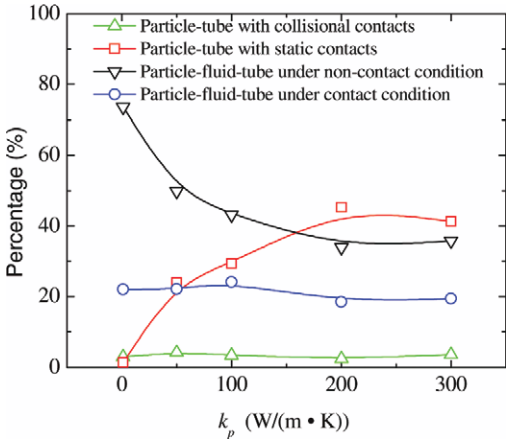

Figure 9. Percentages of heat fluxes in the conduction heat transfer by different conductive mechanisms as a function of k_p when u_{exc} = 0.50 m/s.

[Color figure can be viewed in the online issue, which is available at wileyonlinelibrary.com.]

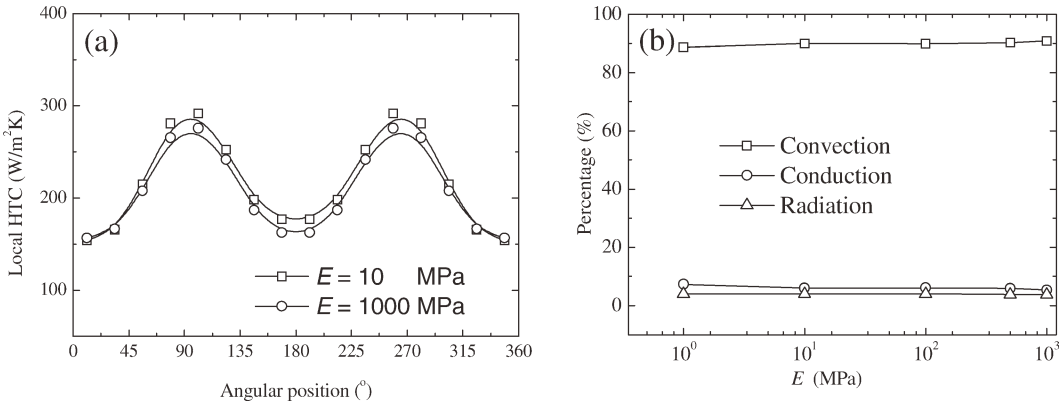

Figure 10. (a) local HTC, and (b) the percentages of heat fluxes by different heat-transfer modes as a function of E when u_{exc} = 0.50 m/s.

and a tube, all the possible mechanisms should be considered.

Effect of the tube temperature T_s

Radiative heat transfer becomes increasingly important with the increase of tube temperature, which increases the environmental temperature of the tube.[1,54] However, information about the heat transfer at high temperatures is scarce in the literature. To address this issue, the heat transfer characteristics of a bubbling fluidized bed at a tube temperature of 600°C are first investigated to establish some general knowledge. Then, the tube temperature is varied in a range of 100–1,500°C to examine its effect on heat transfer.

Figure 12 shows that particles near the high temperature tube will be heated up first, and then they exchange heat with their surrounding particles. Particles are moving vigorously under the influence of the intermittently formed gas bubbles. The falling and rising particles will exchange heat with the tube when they are either close enough to or in contact with the tube. The transfer of heat between particles and tube yields a relatively high-temperature region around the tube.

With the aforementioned definitions, environmental temperature (T_e) and bed temperature (T_b) are obtained to investigate the heat transfer between the bed and the tube. The variations in T_e, T_b and the radiative heat flux q_{rad} with time are shown in Figure 13. T_e is greater than T_b because of the heat region around the tube as shown in Figure 12. T_e is fluctuating significantly due to the intensive heat exchange among particles and the vigorously moving bubbles in the vicinity of the tube. According to the flow and heat-transfer characteristics demonstrated in Figures 1, 3, 4 and 12 and the related discussion, the resulting fluctuation of T_e is rather intrinsic. T_b increases steadily due to the heat transfer from the tube. The temperature difference decreases with the increase of T_e. As a result, the radiative heat fluxes between the tube and the surrounding environment decreases.

The conductive and convective heat fluxes between the bed and the tube also change during the heating-up process. Figure 14 shows that the conductive and convective heat fluxes fluctuate significantly, again as a result of the vigorous motion of particles and gas bubbles around the tube and in the bed. The radiative heat flux decreases steadily with the increase of T_e. The radiative heat transfer is significant with a higher percentage than that of the conductive heat transfer when T_s = 600°C (Figure 14b).

The effect of the surface temperature T_s on the heat transfer characteristic can be quantified by means of the distribution and maximum value of the local HTC, as well as the heat fluxes due to different heat transfer modes. Figure 15a shows that the local HTC increases with an increase in T_s. The distribution of convective HTC remains the same because the fluid flow around the tube does not change

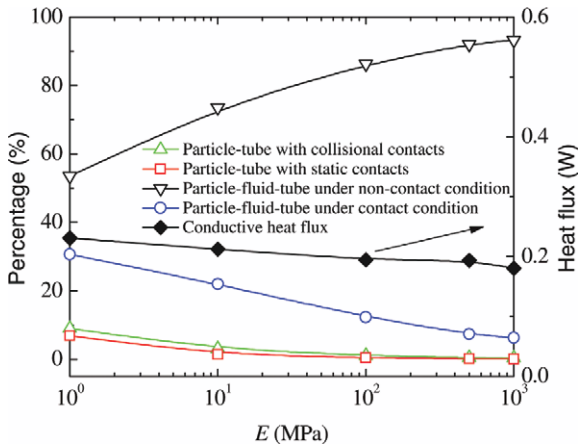

Figure 11. Total conductive heat flux and the percentages of heat fluxes in the conduction heat transfer by different conductive mechanisms as a function of E when u_{exc} = 0.50 m/s.

[Color figure can be viewed in the online issue, which is available at wileyonlinelibrary.com.]

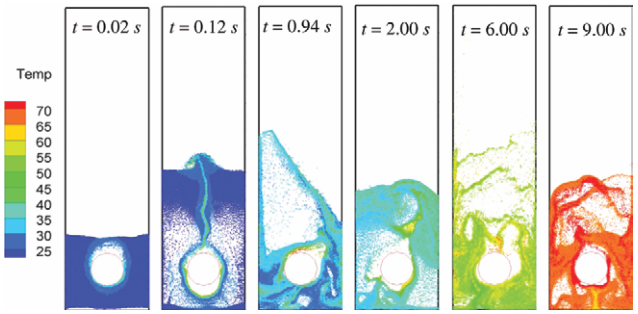

Figure 12. Snapshots of particle flow patterns when T_s = 600°C, where particles are colored by their temperatures.

[Color figure can be viewed in the online issue, which is available at wileyonlinelibrary.com.]

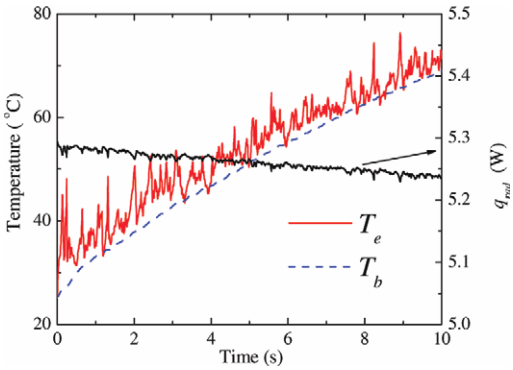

Figure 13. Evolution of T_b, T_e and q_{rad} when T_s = 600°C.

[Color figure can be viewed in the online issue, which is available at wileyonlinelibrary.com.]

much under the influence of T_s. Hence, the general distribution of local HTC, mainly determined by the convective heat transfer mode, changes little, but becomes larger with increasing T_s. The variation of the maximum local HTC of all the sections with T_s is compared with the experimental measurements of Botterill et al.[2] As shown in Figure 15b, good agreement is observed, because of the similar tube geometry and particle properties of the group B type.[55] The small deviations may stem from the small differences in density and diameter of particles. Measurements are not available for temperatures exceeding 800°C, because of the difficulties to conduct experiments at such high temperatures. Nonetheless, the agreement between the measured and simulated results shown in this figure verifies the proposed DPS-CFD approach, particularly the treatments of radiation.

Figure 16 shows the variations of different heat fluxes as a function of T_s. It is clear that the convection is always an important mode of heat transfer under all the conditions considered. The change in the conductive heat flux with T_s is negligible. With the increase of T_s, the difference between T_e and T_b increases. Therefore, the radiative heat flux which varies according to the difference of the fourth power of the temperatures increases more quickly than the convective heat flux which is linear with regard to the temperature difference. The radiative heat flux exceeds the conductive heat flux around T_s = 300°C and then, the convective heat flux around T_s = 1350°C. The results confirm that the radiation is an important heat transfer mode at high tube temperatures. For applications under high temperatures, therefore, factors affecting the radiative heat transfer model should be taken into account to optimize the efficiency and tackle the safety issues.

Conclusions

The combined DPS-CFD approach is extended to study the heat transfer between an immersed horizontal tube and a fluidized bed with group B type of powders. Its validity is

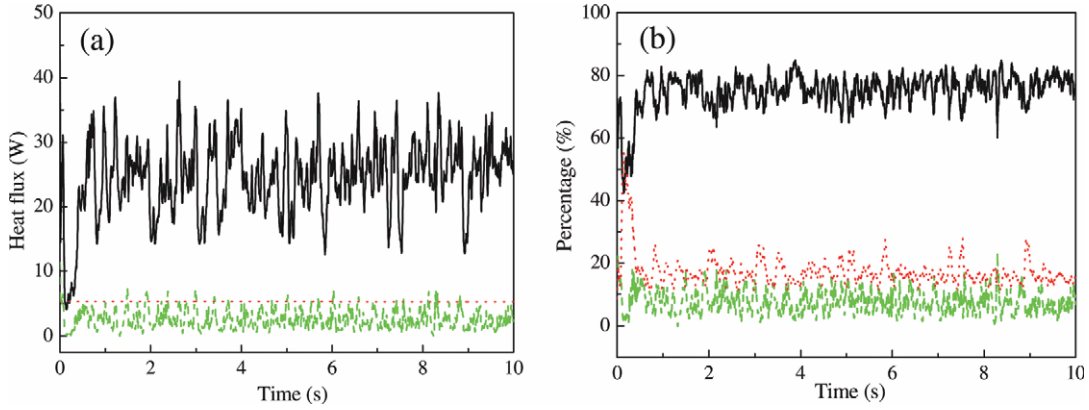

Figure 14. Variations of heat fluxes (a) and their percentages (b) (-, convection; −, conduction; and ..., radiation) when T_s = 600°C.

[Color figure can be viewed in the online issue, which is available at wileyonlinelibrary.com.]

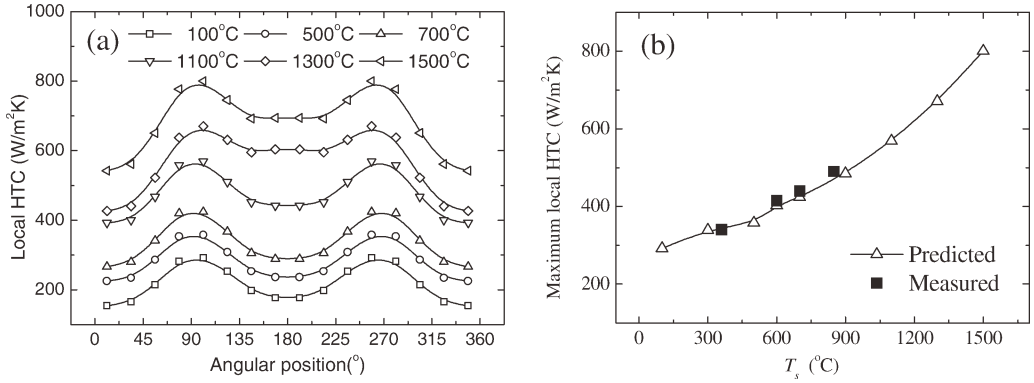

Figure 15. Variations of (a) local HTC, and (b) maximum local HTC at different T_s when u_{exc} = 0.50 m/s.

The measurements are from Botterill et al.[2]

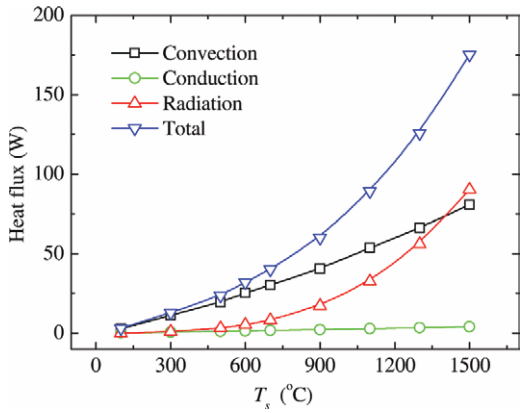

Figure 16. Convective, conductive, radiative and total heat fluxes as a function of T_s when u_{exc} = 0.50 m/s.

[Color figure can be viewed in the online issue, which is available at wileyonlinelibrary.com.]

qualitatively or quantitatively verified, depending on the availability of the measurements in the literature. On this basis, the effects of the following variables are investigated: inlet fluid superficial velocity, particle thermal conductivity, and Young's modulus and tube temperature. The following conclusions can be drawn from this study:

- The non-uniform distribution of the local HTC around an immersed tube can be mechanistically explained in terms of local porosity and contact number which are linked to the local flow patterns. It is shown that the local porosity is large at the sides of a tube and small at upstream and downstream positions. The local HTC is correspondingly large at the sides of the tube and small at upstream and downstream positions. The convective heat transfer plays a dominant role in producing such a non-uniform HTC distribution.
- Inlet fluid superficial velocity affects the heat transfer between a fluidized bed and an immersed tube. The total heat flux increases with the increase of the superficial velocity, while the heat transfer coefficient does not increase consistently. An excessively large inlet superficial velocity can deteriorate the uniformity of the temperature field of the bed, although it can enhance heat transfer. Hence, when selecting the inlet fluid superficial velocity, one should consider the heat transfer capability and the uniformity of temperature field simultaneously for the sake of optimal structural design of a fluidized bed.
- The material properties of particles affect the conductive heat transfer mechanisms, and, hence, the heat transfer between a fluidized bed and an immersed tube. In general, increasing particle thermal conductivity can significantly enhance the conductive heat transfer, while Young's modulus has an insignificant effect. However, the importance of particle properties is very much system-dependent.
- The relative importance of different heat transfer modes is quantified. The convection is always an important heat-transfer mode. Conductive heat transfer is often relatively small, and becomes important under certain conditions, e.g., when particle thermal conductivity is very high. While the radiation is negligible at low temperatures, its importance increases sharply with the increase of the tube temperature. For example, its percentage contribution to the total heat transfer can be as high as the convection at a tube temperature of 1350°C in this study. Radiative heat transfer should be considered for applications at high temperatures.

Acknowledgments

This work has been financially supported by the Australian Research Council. Q. F. Hou is grateful to the University of New South Wales for providing a University Postgraduate Award.

Notation

a, b = constants for the calculation of convective heat flux
A = surface area of a section of the tube, m^2
A_i = surface area of particle i, m^2
A_f = side surface area of a computational cell with unit thickness, m^2
A_w = surface area of wall, m^2
c = coefficient determined by a set of correlations, dimensionless
c_n = normal damping coefficient, dimensionless
c_t = tangential damping coefficient, dimensionless
c_p = representative specific heat capacity of particle, J/(kg·K)
c_{pf} = specific heat capacity of fluid, J/(kg·K)
c_{pi} = representative specific heat capacity of particle i, J/(kg·K)
c_{pj} = representative specific heat capacity of particle j, J/(kg·K)
c_{pt} = specific heat capacity of tube, J/(kg·K)
$C_{d0,i}$ = fluid drag force coefficient on an isolated particle i, dimensionless
C_μ = turbulence model constant (0.09), dimensionless
d_p = particle diameter, m
d_{pi} = particle diameter, m
e = sphere emissivity
e_f = fluid emissivity
E = Young's modulus, Pa
E^* = equivalent Young's modulus, Pa
$\boldsymbol{F}_{fp}$ = volumetric particle-fluid interaction force, N/m^3
$\mathbf{f}_{d,i}$ = particle-fluid drag force on particle i, N
$\mathbf{f}_{d,ij}$ = damping force, N
$\mathbf{f}_{dn,ij}$ = normal damping force, N
$\mathbf{f}_{dt,ij}$ = tangential damping force, N
$\mathbf{f}_{e,ij}$ = elastic force, N
$\mathbf{f}_{en,ij}$ = normal elastic force, N
$\mathbf{f}_{et,ij}$ = tangential elastic force, N
$\mathbf{f}_{pf,i}$ = particle-fluid interaction force on particle i, N
$\mathbf{f}_{pg,i}$ = pressure gradient force, N
$\mathbf{f}_{t,ij}$ = Coulomb friction force, N
$\boldsymbol{g}$ = gravitational acceleration, m/s^2
h = heat transfer coefficient, $W/(m^2·K)$
$\boldsymbol{I}_i$ = moment of the inertia of particle i, $kg·m^2$
k = turbulent kinetic energy, m^2/s^2
k_e = effective thermal conductivity, W/(m·K)
k_f = fluid thermal conductivity, W/(m·K)
k_p = thermal conductivity of particle, W/(m·K)
k_{pi} = thermal conductivity of particle i, W/(m·K)
k_{pj} = thermal conductivity of particle j, W/(m·K)
k_{pt} = thermal conductivity of the tube, W/(m·K)
k_V = number of particles in a computational cell, dimensionless
k_Ω = number of particles in a domain Ω, dimensionless
L = characteristic length of wall, m
m_i = mass of particle i, kg
m_{ij} = equivalent mass of particles in contact, kg
M = molar mass (0.029 for air), kg/mol
N = number of particles in a bed, dimensionless
$\boldsymbol{n}$ = unit normal vector at contact
p = fluid pressure, Pa
P = absolute pressure (= 101325), Pa
Pr = Prandtl number ($c_{pf}\mu_f/k_f$), dimensionless
q_{cond} = conductive heat flux, W
q_{conv} = convective heat flux, W
$q_{f,rad}$ = radiative heat flux between fluid and surrounding environment, W
$q_{i,j}$ = conductive heat flux between particles i and j, W
$q_{i,f}$ = convective heat flux between particle i and surrounding fluid, W
$q_{i,rad}$ = radiative heat flux between particle i and surrounding environment, W
$q_{i,wall}$ = conductive heat flux between particles i and a wall, W
$q_{i,tube}$ = conductive heat flux between particles i and a tube, W
q_{rad} = radiative heat flux, W
Q = volumetric heat flux, J/m^3

R = universal gas constant (= 8.314), J/(mol·K)
R_i, R_j = radius of particle i, m
$\boldsymbol{R}_i$, $\boldsymbol{R}_j$ = vector of the mass center of the particle to contact plane, m
$\boldsymbol{R}_{ij}$ = vector of the mass center of the particles i and j at contact, m
R^* = equivalent particle radius, m
r_c = particle–particle contact radius, m
Re_i = particle Reynolds number, dimensionless
T_i, T_j = representative temperature of particles i and j, K
T_b = bed temperature, K
T_e = environmental temperature of the tube, K
T_f = temperature of fluid, K
$T_{f,\Omega}$ = local temperature of fluid, K
$T_{\text{local},i}$ = environmental temperature of particle i, K
T_s = surface temperature of the tube, K
$\boldsymbol{T}_{r,ij}$ = rolling friction torque, N/m
$\boldsymbol{T}_{t,ij}$ = torque by tangential force, N/m
t = time, s
Δt = time step, s
t_c = time of particle–particle collision, s
t_d = time of particle–particle contact duration, s
$\boldsymbol{u}$ = local fluid velocity, m/s
$\boldsymbol{u}_i$ = local fluid velocity, m/s
u = inlet fluid superficial velocity, m/s
u_{exc} = excess fluid velocity, defined by $u_{\text{exc}} = u - u_{mf}$, m/s
u_{mf} = minimum fluidization velocity, m/s
$\mathbf{v}_i$ = particle translational velocity, m/s
$\mathbf{v}_{ij}$ = relative particle velocity, m/s
$\mathbf{v}_{n,ij}$ = normal relative velocity of particles i and j, m/s
$\mathbf{v}_{t,ij}$ = tangential relative velocity of particles i and j, m/s
V_i = volume of a particle or part of the volume, m^3
ΔV = volume of a computational cell, m^3
Z = tube position, m

Greek letters

δ_k = Kronecker delta, dimensionless
δ_n = relative normal displacement at contact, m
δ_t = relative tangential displacement at contact, m
$\hat{\delta}_t$ = unit vector of δ_t
$\delta_{t,\max}$ = maximum of δ_t when the particles start to slide, m
ϵ = dissipation rate of turbulent kinetic energy, m^2/s^3
ϵ_f = porosity, dimensionless
ϵ_i = local porosity, dimensionless
μ_e = fluid effective viscosity, kg/(m·s)
μ_f = fluid molecular viscosity, kg/(m·s)
μ_r = rolling friction coefficient, dimensionless
μ_s = sliding friction coefficient, dimensionless
μ_t = fluid turbulent viscosity, kg/(m·s)
ν = Poisson ratio, dimensionless
ρ_p = density of particle, kg/m^3
ρ_{pi} = density of particle i, kg/m^3
ρ_{pj} = density of particle j, kg/m^3
ρ_f = fluid density, kg/m^3
σ = Stefan-Boltzmann constant, $W/(m^2 \cdot K^4)$
σ_T = turbulence Prandtl number, dimensionless
τ = stress tensor, Pa
ω_i = angular velocity of particle i, 1/s
ω_{ij}^n = the component of the relative angular velocity in contact plane, 1/s
$\hat{\omega}_{ij}^n$ = unit vector of ω_n, 1/s

Subscripts

b = bed
d = damping
e = elastic/effective/environmental
f = fluid
i = particle i
ij = between particles i and j
j = particle j
n = normal component
p = particle
r = rolling
t = tangential component/turbulent/tube
w = wall

Abbreviation

CN = coordination number
cond = conduction
conv = convection
exc = excess
HTC = heat transfer coefficient
rad = radiation
Temp = temperature

Literature Cited

1. Chen JC, Grace JR, Golriz MR. Heat transfer in fluidized beds: design methods. *Powder Technol*. 2005;150:123–132.
2. Botterill JSM, Teoman Y, Yuregir KR. Factors affecting heat transfer between gas-fluidized beds and immersed surfaces. *Powder Technol*. 1984;39:177–189.
3. Kunii D, Levenspiel O. *Fluidization Engineering*. Boston: Butterworth-Heinemann; 1991.
4. Molerus O, Wirth KE. *Heat Transfer in Fluidized Beds*. London: Chapman and Hall; 1997.
5. Wakao N, Kaguei S. *Heat and Mass Transfer in Packed Beds*. New York: Gordon and Breach Science Publishers; 1982.
6. Gelperin NI, Einstein VG, eds. *Heat Transfer in Fluidized Beds*. London: Academic Press; 1971. Davidson JF, Harrison D, eds. Fluidization.
7. Collier AP, Hayhurst AN, Richardson JL, Scott SA. The heat transfer coefficient between a particle and a bed (packed or fluidised) of much larger particles. *Chem Eng Sci*. 2004;59:4613–4620.
8. Parmar MS, Hayhurst AN. The heat transfer coefficient for a freely moving sphere in a bubbling fluidised bed. *Chem Eng Sci*. 2002;57:3485–3494.
9. Prins W, Draijer W, van Swaaij WPM. Heat transfer to immersed spheres fixed or freely moving in a gas-fluidized bed. *20th Proceedings of the International Centre for Heat and Mass Transfer*: Washington: Hemisphere; 1985:317–331.
10. Scott SA, Davidson JF, Dennis JS, Hayhurst AN. Heat transfer to a single sphere immersed in beds of particles supplied by gas at rates above and below minimum fluidization. *Ind Eng Chem Res*. 2004;43:5632–5644.
11. Kim SW, Ahn JY, Kim SD, Lee DH. Heat transfer and bubble characteristics in a fluidized bed with immersed horizontal tube bundle. *Int J Heat Mass Transfer*. 2003;46:399–409.
12. Wong YS, Seville JPK. Single-particle motion and heat transfer in fluidized beds. *AIChE J*. 2006;52:4099–4109.
13. Masoumifard N, Mostoufi N, Hamidi A-A, Sotudeh-Gharebagh R. Investigation of heat transfer between a horizontal tube and gas-solid fluidized bed. *Int J Heat Fluid Flow*. 2008;29:1504–1511.
14. Zhu HP, Zhou ZY, Yang RY, Yu AB. Discrete particle simulation of particulate systems: A review of major applications and findings. *Chem Eng Sci*. 2008;63:5728–5770.
15. Zhu HP, Zhou ZY, Yang RY, Yu AB. Discrete particle simulation of particulate systems: Theoretical developments. *Chem Eng Sci*. 2007;62:3378–3396.
16. Kaneko Y, Shiojima T, Horio M. DEM simulation of fluidized beds for gas-phase olefin polymerization. *Chem Eng Sci*. 1999;54:5809–5821.
17. Zhou ZY, Yu AB, Zulli P. Particle scale study of heat transfer in packed and bubbling fluidized beds. *AIChE J*. 2009;55:868–884.
18. Malone KF, Xu BH. Particle-scale simulation of heat transfer in liquid-fluidised beds. *Powder Technol*. 2008;184:189–204.
19. Zhou HS, Flamant G, Gauthier D. DEM-LES simulation of coal combustion in a bubbling fluidized bed Part II: coal combustion at the particle level. *Chem Eng Sci*. 2004;59:4205–4215.
20. Di Maio FP, Di Renzo A, Trevisan D. Comparison of heat transfer models in DEM-CFD simulations of fluidized beds with an immersed probe. *Powder Technol*. 2009;193:257–265.
21. Zhao YZ, Jiang MQ, Liu YL, Zheng JY. Particle-scale simulation of the flow and heat transfer behaviors in fluidized bed with immersed tube. *AIChE J*. 2009;55:3109–3124.
22. Feng YQ, Yu AB. Effect of bed thickness on segregation behaviour of particle mixtures in a gas fluidized bed. *Ind Eng Chem Res*. 2010;49:3459–3468.
23. Botterill JSM, Teoman Y, Yuregir KR. Minimum fluidization velocity at high temperatures-comment. *Ind Eng Chem Proc Des Dev*. 1982;21:784–785.
24. Pattipati RR, Wen CY. Minimum fluidization velocity at high temperatures-response. *Ind Eng Chem Proc Des Dev*. 1982;21:785–786.
25. Flamant G, Arnaud G. Analysis and theoretical study of high-temperature heat transfer between a wall and a fluidized bed. *Int J Heat Mass Transfer*. 1984;27:1725–1735.

26. Chung TY, Welty JR. Tube array heat transfer in fluidized beds- A study of particle size effects. *AIChE J*. 1989;35:1170–1176.
27. Chen JC, Chen KL. Analysis of simultaneous radiative and conductive heat-transfer in fluidized-beds. *Chem Eng Commun*. 1981;9:255–271.
28. Hou QF, Zhou ZY, Yu AB. Investigation of heat transfer in bubbling fluidization with an immersed tube. *6th International Symposium on Multiphase Flow, Heat Mass Transfer and Energy Conversion*. Xi'an, China, July 2009.
29. Cundall PA, Strack ODL. A discrete numerical-model for granular assemblies. *Géotechnique*. 1979;29:47–65.
30. Xu BH, Yu AB. Comments on the paper: Numerical simulation of the gas-solid flow in a fluidized bed by combining discrete particle method with computational fluid dynamics- reply. *Chem Eng Sci*. 1998;53:2646–2647.
31. Zhou ZY, Kuang SB, Chu KW, Yu AB. Discrete particle simulation of particle-fluid flow: Model formulations and their applicability. *J Fluid Mech*. 2010;661:482–510.
32. Incropera FP, Dewitt DP. *Fundamentals of Heat and Mass Transfer*. 5th ed. New York: John Wiley & Sons; 2002.
33. Zhou ZY, Yu AB, Zulli P. A new computational method for studying heat transfer in fluid bed reactors. *Powder Technol*. 2010;197:102–110.
34. Delvosalle C, Vanderschuren J. Gas-to-particle and particle-to-particle heat transfer in fluidized beds of large particles. *Chem Eng Sci*. 1985;40:769–779.
35. Cheng GJ, Yu AB, Zulli P. Evaluation of effective thermal conductivity from the structure of a packed bed. *Chem Eng Sci*. 1999;54:4199–4209.
36. Batchelor GK, O'Brien RW. Thermal or electrical conduction through a granular material. *Proc R Soc London A*. 1977;355:313–333.
37. Sun J, Chen MM. A theoretical analysis of heat transfer due to particle impact. *Int J Heat Mass Transfer*. 1988;31:969–975.
38. Zhou JH, Yu AB, Horio M. Finite element modeling of the transient heat conduction between colliding particles. *Chem Eng J*. 2008;139:510–516.
39. Gidaspow D. *Multiphase Flow and Fluidization*. San Diego: Academic Press; 1994.
40. Launder BE, Spalding DB. The numerical computation of turbulent flows. *Comput Methods Appl Mech Eng*. 1974;3:269–289.
41. Zhang SJ, Yu AB, Zulli P, Wright B, Tüzün U. Modelling of the solids flow in a blast furnace. *ISIJ Int*. 1998;38:1311–1319.
42. Kuang SB, Yu AB. Micromechanic modelling and analysis of the flow regimes in horizontal pneumatic conveying. *AIChE J*. 2010. doi:10.1002/aic.12480.
43. Xu BH, Yu AB. Numerical simulation of the gas-solid flow in a fluidized bed by combining discrete particle method with computational fluid dynamics. *Chem Eng Sci*. 1997;52:2785–2809.
44. Feng YQ, Xu BH, Zhang SJ, Yu AB, Zulli P. Discrete particle simulation of gas fluidization of particle mixtures. *AIChE J*. 2004;50:1713–1728.
45. Shi D, Vargas WL, McCarthy JJ. Heat transfer in rotary kilns with interstitial gases. *Chem Eng Sci*. 2008;63:4506–4516.
46. Rong DG, Mikami T, Horio M. Particle and bubble movements around tubes immersed in fluidized beds - a numerical study. *Chem Eng Sci*. 1999;54:5737–5754.
47. Mickley HS, Trilling CA. Heat transfer characteristics of fluidized beds. *Ind Eng.Chem*. 1949;41:1135–1147.
48. Chandran R, Chen JC. Bed-surface contact dynamics for horizontal tubes in fluidized beds. *AIChE J*. 1982;28:907–914.
49. Glass DH, Harrison D. Flow patterns near a solid obstacle in a fluidized bed. *Chem Eng Sci*. 1964;19:1001–1002.
50. Dong KJ, Yang RY, Zou RP, An XZ, Yu AB. Critical states and phase diagram in the packing of uniform spheres. *Europhys Lett*. 2009;86:46003.
51. Yang RY, Zou RP, Yu AB. Computer simulation of the packing of fine particles. *Phys Rev E*. 2000;62:3900–3908.
52. Schmidt A, Renz U. Numerical prediction of heat transfer between a bubbling fluidized bed and an immersed tube bundle. *Heat Mass Transfer*. 2005;41:257–270.
53. Kennedy TC, Donovan JE, Trigas A. Forces on immersed tubes in fluidized beds. *AIChE J*. 1981;27:351–357.
54. Mathur A, Saxena SC. Total and radiative heat transfer to an immersed surface in a gas-fluidized bed. *AIChE J*. 1987;33:1124–1135.
55. Geldart D. Types of gas fluidization. *Powder Technol*. 1973;7:285–292.

Manuscript received Dec. 5, 2010, revision received Apr. 13, 2011, and final revision received Jun. 2, 2011.